TEKTONIKA

Laboratory Simulation of Earthquake-Induced Damage in Lava Dome Rocks

Lauren N. Schaefer [*1,2], **Jackie E. Kendrick** [3,4], **Yan Lavallée** [3,4], **Jenny Schauroth** [4], **Oliver D. Lamb** [4,5], **Anthony Lamur** [3,4], **Takahiro Miwa** [6], **Ben M. Kennedy** [2]

[1]U.S. Geological Survey, Geologic Hazards Science Center, 1711 Illinois St., Golden, CO, 80401, USA | [2]School of Earth and Environment, University of Canterbury, Christchurch, 8140, New Zealand | [3]Department of Earth and Environmental Sciences, Ludwig Maximilian University of Munich, Munich 80333, Germany | [4]Department of Earth, Ocean and Ecological Sciences, University of Liverpool, Liverpool, L69 3GP, UK | [5]GNS Science, Wairakei Research Centre, Taupō, 3384, New Zealand | [6]National Research Institute for Earth Science and Disaster Resilience (NIED), Tsukuba, Japan

Abstract Earthquakes can impart varying degrees of damage and permanent, inelastic strain on materials, potentially resulting in ruptures that may promote hazards such as landslides and other collapse events. However, the accumulation of damage in rocks under the frequency and amplitude of shaking experienced during earthquake events is rarely systematically measured due to technical limitations. Here, we characterize damage evolution during laboratory experiments on a suite of dacitic rocks from Unzen volcano, Japan, to help resolve accumulated damage and landslide susceptibility of lava domes during regional earthquake events. Damage was imparted during slow (time-dependent creep) and fast (stress-oscillation earthquake simulations) uniaxial loading in compression and tension. Damage evolution is approximated from strain during experiments; all samples accumulate strain during earthquake events, but microfracture-dominated samples tend to be more susceptible to damage than vesicle-dominated samples. The orientation of existing fabrics with respect to loading direction dictates the magnitude of strain accumulation under load oscillations. During each "earthquake" experiment of multiple dynamic stress-oscillations, samples accumulate inelastic strain. The strain imparted during each successive event is initially high and then reduces after 5-7 events, except when stressing results in failure. The strain rate during phases of intermittent stressing tends to be higher than prior to them. Understanding the accumulation of damage and the potential for brittle failure of rocks subjected to earthquakes can help define the origin and timing of certain landslides, rockfalls, lava dome collapses, and other failure events.

Executive Editor:
Craig Magee
Associate Editor:
Noah Phillips
Technical Editor:
Mohamed Gouiza

Reviewers:
Michael Heap
Holly Unwin

Submitted:
1 July 2022
Accepted:
14 April 2023
Published:
22 May 2023

1 Introduction

Volcanic edifices and structures such as lava domes are particularly prone to both structural and mechanical instability, as they are unconfined structures often sitting atop a weak basement (*Borgia et al.*, 1992). They can experience relatively rapid growth (*Yamamoto et al.*, 1993), and are subject to magmatic (*Kerr*, 1984) and hydrothermal activity (including mineral alteration; *Ball et al.*, 2015) as well as earthquake loading (*Belousov*, 1995; *Walter et al.*, 2007) that may decrease volcanic slope stability. Volcanic domes can fail in both compression and tension. Compressional failures are related to gravitational forces on the dome interior due to dome growth, in addition to gas and magma pressure (*Voight*, 2000). Tensile failure is most relevant to exterior parts of the dome. For example, emplacement on slopes, bulging of a dome, or pressurized gases within the pores can result in extensional stresses that cause rocks to fail in tension (*Sato et al.*, 1992; *Voight*, 2000; *Hornby et al.*, 2019). If they become unstable, collapse may lead to dangerous rockfalls, debris avalanches, and pyroclastic density currents (e.g., *Calder et al.*, 2002); in extreme cases, they may lead to large sector collapses (*Kerr*, 1984; *Walter et al.*, 2019).

Volcanoes are often located near plate boundaries and are subjected to both tectonic and volcanic earthquakes, both of which are known to trigger landslide events (*Saito et al.*, 2018; *Thouret et al.*, 1990). Dynamic stress perturbations from earthquakes can deform rock and prompt the nucleation, growth, and coalescence of cracks or fractures. This can lead to stress field changes around volcanoes (*Farías and Basualto*, 2020; *Fujita et al.*, 2013) and can trigger additional earthquakes at volcanoes (*Bell et al.*, 2021; *Enescu et al.*, 2016). Mechanical weakening of rock and granular material due to earthquakes has been measured at several volcanoes (e.g., *Brenguier et al.*, 2014; *Lesage et al.*, 2014; *Yates et al.*, 2019). Understanding the degree of damage volcanic rocks may experience during earthquakes, which contributes to understanding the likelihood and timing of material failure, can aid in hazard mitigation at volcanoes.

*✉ lschaefer@usgs.gov

Experimental rock physics has greatly expanded our understanding of rock mechanics and failure, including fault frictional strength (*Scholz*, 1968; *Attewell and Farmer*, 1973; *Scholz and Koczynski*, 1979; *Rutter*, 1986; *Schultz*, 1995; *Marone*, 1998; *Eberhardt et al.*, 1999; *Lockner and Beeler*, 2002; *Paterson and Wong*, 2005; *Cerfontaine and Collin*, 2018; *Liu and Dai*, 2021). The mechanical behavior and failure modes (i.e., brittle versus ductile) of volcanic rock differ depending on the extent and rate of stress applied, along with the confining pressure, temperature, and saturation conditions (e.g., *Heap and Violay*, 2021; *Lavallée and Kendrick*, 2021). During stressing events, rocks deform elastically to a critical yield point, after which cracks nucleate and propagate and the rock deforms inelastically. Eventually, cracks may coalesce, resulting in failure (e.g., *Klein and Reuschlé*, 2004). During prolonged and constant stressing conditions (e.g., gravitational stress), rock may deform inelastically and eventually fail due to sub-critical crack growth and coalescence, a phenomenon known as time-dependent brittle creep (*Brantut et al.*, 2013). Typically, rock mechanics experimentation is conducted under relatively slow (e.g., typically 10–5 s^{-1} for compressive strength tests following guidance from *ASTM*, 2014) and/or constant loading rates, which do not reflect the rates of earthquake loading. Investigations of cyclic/fatigue loading of rock, which apply constant or variable stress amplitudes, show that the accumulation of damage with each stressing cycle can eventually lead to failure (*Cerfontaine and Collin*, 2018). However, these tests often do not capture the frequency range and amplitude conditions that rocks experience during earthquake events, such as waveforms with amplitudes that increase and decrease over time. Additionally, laboratory experiments have rarely considered tensile deformation, which is of vital importance to failure in low-confinement scenarios (e.g., *Diederichs*, 2003, and references therein) such as volcanic edifices, non-volcanic slopes in mountainous regions, and lava domes.

Recently, *Lamur et al.* (2023) investigated damage accumulation and weakening caused by repeating stress oscillations on porphyritic andesite and found that stress oscillations impart more damage than constant loads, resulting in higher fracture densities in post-experimental rock samples and occasionally prompting sample failure. Here, we expand on these earlier studies by experimentally simulating and quantifying the impact of dynamic repeated stressing events (e.g., earthquakes) on dacitic volcanic rocks loaded uniaxially, in compression and tension. We use porous dacite from Mt. Fugen, of the Unzen-dake volcanic complex (referred to as 'Unzen', Figure 1) in Japan. The recently emplaced lava dome complex exists on a steep slope, and the east side of the lava dome shows signs of structural instability (*Satou et al.*, 2014; *Hirakawa et al.*, 2018; *Shi et al.*, 2018), which may be exacerbated by earthquake activity (e.g., *Voight et al.*, 1981; *Voight*, 2000; *Walter et al.*, 2007; *Wallace et al.*, 2021). Such a prospect has historically occurred at Unzen volcano, where a lava dome collapsed and generated a large tsunami that caused 15,000 casualties during the 1792 M6.4 Shimabara-Shigatusaku earthquake (*Inoue*, 1999). Damage measured in laboratory experiments can help inform accumulated damage and landslide susceptibility of lava domes during earthquake events.

2 Mt. Unzen Lava Dome Growth and Structural Instability

Mt. Fugen of the Unzen-dake volcanic complex in southwestern Japan (Figure 1) began erupting on 17 November 1990 after 198 years of quiescence (*Nakada et al.*, 1999). Magma erupted effusively between May 1991 and February 1995; 2.1 × 108 m^3 of lava (dense-rock equivalent) erupted, constructing the Heisei-Shinzan dome complex (*Nakada et al.*, 1999). The dome represents approximately half of the erupted volume, measuring 1.2 km (east-west) long by 0.8 km (north-south) wide at its maximum size and it comprises a series of 13 blocky lava lobes, many of which have been buried by successive lobes (Figure 1 *Nakada et al.*, 1999). The remainder of the material was shed as pyroclastic density currents (PDCs) and rockfalls as the dome went through repeating cycles of growth and partial collapse during several transitions in eruptive intensity and style (*Nakada and Motomura*, 1999). In total, over 9,400 PDCs occurred from dome collapses *Miyabuchi* (1999), extending up to 5.5 km down the valleys to the north, east and south of the volcano *Yamamoto et al.* (1993), causing the deaths of 44 people, evacuation of 11,000 people, and destruction of approximately 800 buildings *Nakada et al.* (1999).

Deformation of the dome and flank lobes has occurred since activity ceased in February 1995. Monitoring using global positioning system (GPS) equipment and electronic distance measurements (EDMs) from 1996 to 1999 found the largest displacement parallel in the direction of the steepest slope, indicating that the lobes were still hot and viscously deforming *Matsushima and Takagi* (2000). Electro-optical distance measurements (EDM) show that between 1997 and 2011, Lobe 11 (Figure 1) had advanced over 1 m in 14 years, or 70 mm/year (*Kohashi et al.*, 2012). Between 2007 and 2014, EDM and ground-based synthetic aperture radar measured non-uniform east-south movement of Lobe 11B with displacements between 25–65 mm/year, which was attributed to differences in the deformability of the materials underlying Lobe 11B (*Satou et al.*, 2014). Lasting heat sources are also evident from ongoing fumarolic activity that has continued to the present day (Figure 1e; *Hashimoto et al.*, 2020), causing local thermal and chemical alteration (*Almberg et al.*, 2008) that could contribute to instability via mechanical weakening of material as primary minerals transform into weaker secondary products such as clay minerals (e.g., *Ball et al.*, 2015). At the time of writing, the risk of collapse of Lobe 11 is considered high by the Committee of

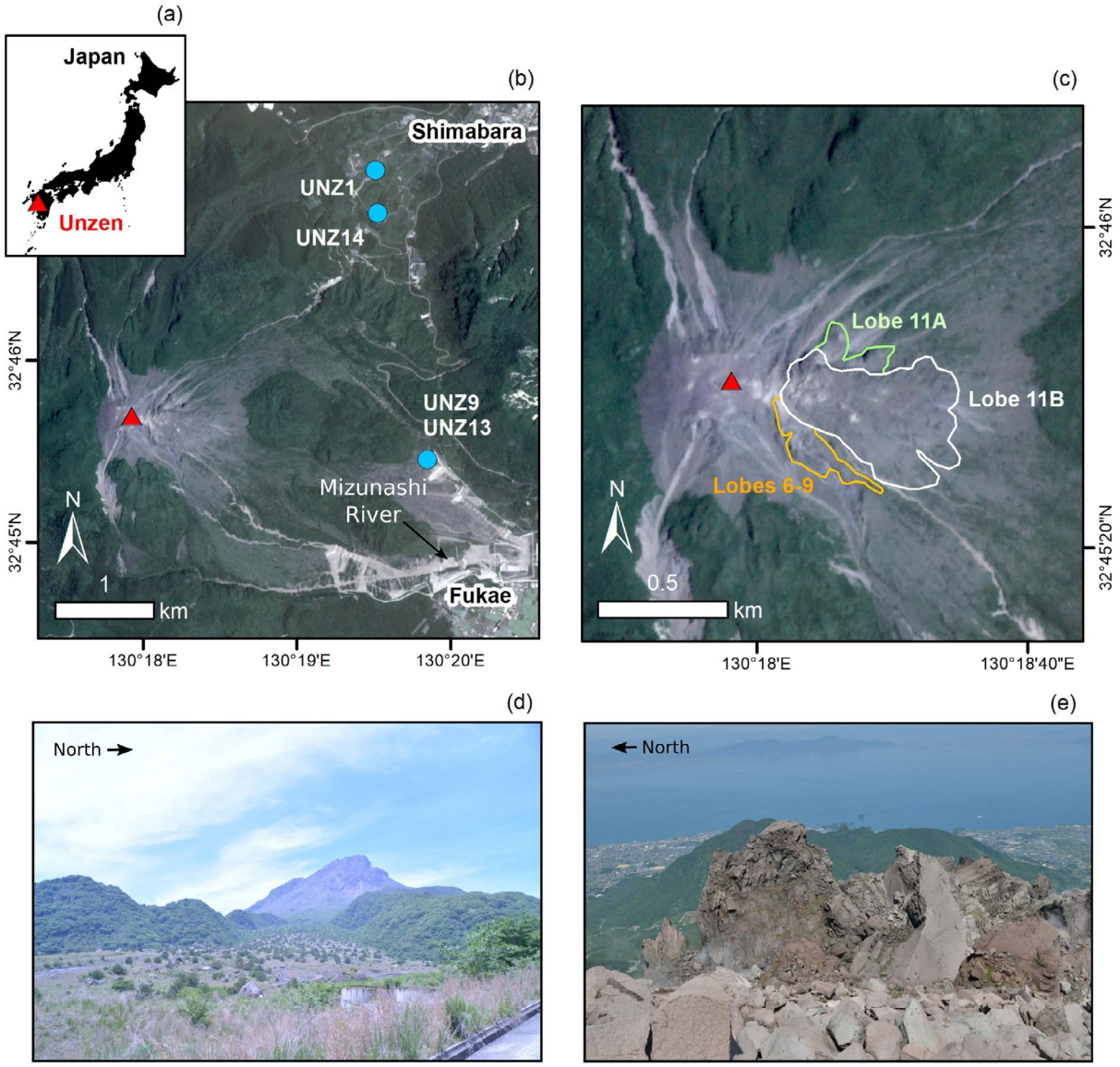

Figure 1 – Location of Unzen volcano, the lava dome, and blocks used in the study. **(a)** Location of Unzen in Japan. Red triangle indicates the summit of the dome in this and other figure parts. **(b)** Location of blocks UNZ1, UNZ9, UNZ13, and UNZ14. **(c)** Outlined trace of the lava dome lobes, including Lobes 6–9 (undifferentiated), 11A, and 11B, as outlined in *Satou et al.* (2014). Multispectral PlanetScope image from 7 June 2020. Image acquired by © Planet 2020. **(d)** View of the steep-sided lava dome looking west-northwest up the valley from the collection site of samples UNZ9 and UNZ13 in 2016. Photograph used with permission, courtesy of R. Coats. **(e)** The view from the summit of the lava dome looking east over lobe 11 in the foreground, with the city of Shimabara and the Ariake Sea in the distance. Steam in the foreground is evidence of ongoing fumarolic activity. Photo by Y. Lavallée.

Survey and Countermeasure on Lava Dome Collapse in Mt. Unzen, and an exclusion zone remains active to the east of the summit. The blocky nature of the lava dome, emplacement of the dome on a steep slope, a weak substrate, ongoing alteration, and ongoing and uneven downslope deformation are all factors that could contribute to the complete or partial collapse of the lobe. In the case of complete collapse, modeling indicates a maximum block-and-ash flow volume of 1.46 x 107 m^3, which could travel 8.5 km at an average velocity of 20 m/s (*Shi et al.*, 2018). This hazard prompted experimental studies of the Unzen dome lavas to better characterize this hazard (*Coats et al.*, 2018; *Cordonnier et al.*, 2009; *Hornby et al.*, 2015; *Kendrick et al.*, 2021; *Schaefer et al.*, 2020; *Scheu et al.*, 2008).

3 Materials and Methodology

3.1 Materials and Apparatus

Four blocks of porphyritic dacite were collected from pyroclastic deposits of Unzen volcano to prepare specimens for this study, as they span the range of physical properties (primarily porosity of approximately 10–35%) generated during the Heisei-Shinzan dome eruption (cf. *Kueppers et al.*, 2005). Sample blocks include UNZ1 (average total porosity (ϕ) of 18.6%; *Kendrick et al.*, 2021) and UNZ14 (ϕ = 13.4%) collected from the June 1993 block-and-ash flow deposits in the Minami-Senbongi area; and block UNZ9 (ϕ = 16.2%) and UNZ13 (ϕ = 29%) collected with permission from the May–August 1991 deposits in the

restricted area of the Mizunashi River (Figure 1). The rocks are porphyritic dacite (~63 wt% SiO2) with large (>3 mm) and abundant (>25 vol%) plagioclase phenocrysts, with lower proportions of amphibole, biotite, and quartz phenocrysts set in a partially crystalline groundmass of plagioclase, pyroxene, quartz pargasite and Fe-Ti oxides in a rhyolitic interstitial glass (*Coats et al.*, 2018; *Kendrick et al.*, 2021). The rock samples are equivalent to lavas found in situ in the dome (e.g., *Nakada and Motomura*, 1999; *Wallace et al.*, 2019).

The main distinctions between the four blocks chosen for this study relate to their porosity and pore geometry (Figure 2). UNZ1 has a mid to high porosity (of the samples selected) of 18.6%. Pores consist of irregular-shaped vesicles distributed evenly throughout, typically adjacent to large plagioclase phenocrysts, as well as microfractures that pass through phenocrysts and groundmass alike (often >3mm). UNZ9 has an anisotropic cataclastic fabric of dense and porous bands, with an average porosity of 16.2% (the second lowest of the samples selected). The pores are elongate, sub-angular voids flanked by a granular fault gouge of angular broken crystals and groundmass. Due to the anisotropy of this block, UNZ9 was cored parallel to the banding to produce sample UNZ9a, and perpendicular to make UNZ9b (see Figure SI-1, Supporting Information), i.e., horizontally and vertically in the thin section image (Figure 2), respectively. This allowed us to explore the effect of the banding on the mechanical behavior. UNZ13 has the highest porosity of all the samples at 29.0%, and has a greater percentage of larger pores (>5 mm) compared to the other samples. Most of its pores are large, sub-rounded vesicles, which are adjacent to euhedral phenocrysts, and the glassy groundmass also contains common small sub-rounded vesicles that have a slight local preferred orientation which varies in proximity to large phenocrysts. UNZ14 has the lowest porosity of just 13.4%, with small, sub-rounded vesicles unevenly distributed within the sample, adjacent to phenocrysts that are frequently broken and contain hairline fractures. Less common microfractures are also present in the groundmass of UNZ14. The physical and mechanical properties of the blocks are fully characterized by *Kendrick et al.* (2021) and *Coats et al.* (2018) and follow the same naming convention as these publications.

Experiments were carried out in the Experimental Volcanology and Geothermal Research Laboratory at the University of Liverpool. Loading experiments were carried out in a 100 kN Instron 8800 uniaxial press at room temperature using both compression tests, and Brazilian disk tests to provide the indirect tensile strength (hereafter referred to as tensile strength/tension tests). Load was recorded by an Instron Dynacell 2527 load cell at 100 Hz, which has an accuracy of ± 0.1% of the full load capacity (100 kN). Strain is recorded using an Instron LVDT (Linear Variable Differential Transformer) Deflection Sensor, which has an accuracy of ±0.00001 mm or ±0.05% of the measured displacement, whichever is the largest. For the compression tests, cylindrical specimens with a 20 mm diameter were cored and then cut to a length of 40 mm to form cylinders with a 2:1 length:diameter ratio. The cylinders were axially compressed between two parallel plates in the loading frame during testing. For the Brazilian tests, cylindrical specimens with a 40 mm diameter were cored and then cut to a length of 20 mm to form disks with a 2:1 diameter:length ratio. The disks were diametrically compressed between two parallel plates in the loading frame to induce tensional stresses in the orthogonal direction. The specimen dimensions and loading frame setup follow American Society for Testing and Material (ASTM) standards for unconfined (uniaxial) compression and Brazil tensile strength testing (ASTM Standard D7012 (*ASTM*, 2014) and ASTM Standard D3967 (*ASTM*, 2016), respectively). Each core and disk was used only once, even if the sample survived the imposed conditions. Following preparation, specimens were oven dried at 60°C for 24 hours and then placed into a vacuum chamber for one week prior to porosity and permeability measurements and mechanical experiments.

Prior to testing, the connected porosity of all the prepared specimens were determined using an Accupyc 1340 helium pycnometer, and the permeability was determined using a TinyPerm II Permeameter from New England Research Inc.; details of these methods and results are published in *Kendrick et al.* (2021). Table 1 provides a description of the specimens used in load hold and load oscillation experiments in this study.

3.2 Experimental Methods

In this study, we aim to experimentally simulate the effects of earthquakes on volcanic rocks, quantify the resulting damage in the form of inelastic strain, and describe any patterns as a function of rock properties (e.g., porosity or textural anisotropy). Our experiments are designed to mimic the quasi-uniaxial stress conditions expected in a lava dome (near-surface, largely unconfined) during and between earthquakes. We do so in two steps: First, to characterize the mechanical properties and physical evolution of rock subjected to prolonged loading, we subject rock specimens to load-hold periods and study their resultant changes during creep (see details in Section 3.2.1). Second, we load another set of rock specimens to a sub-critical load (stress) and subject them to regular stress oscillations to simulate elastic waves propagating from earthquake sources (see details in Section 3.2.2). We then proceed to assess the evolution of damage during earthquake events using the accumulation of inelastic strain and changes in strain rate as a proxy. Because damage (accumulated inelastic strain) was measured during load holds before and after earthquake events, keeping specimens below the critical stress necessary for creep, as determined from creep experiments, was

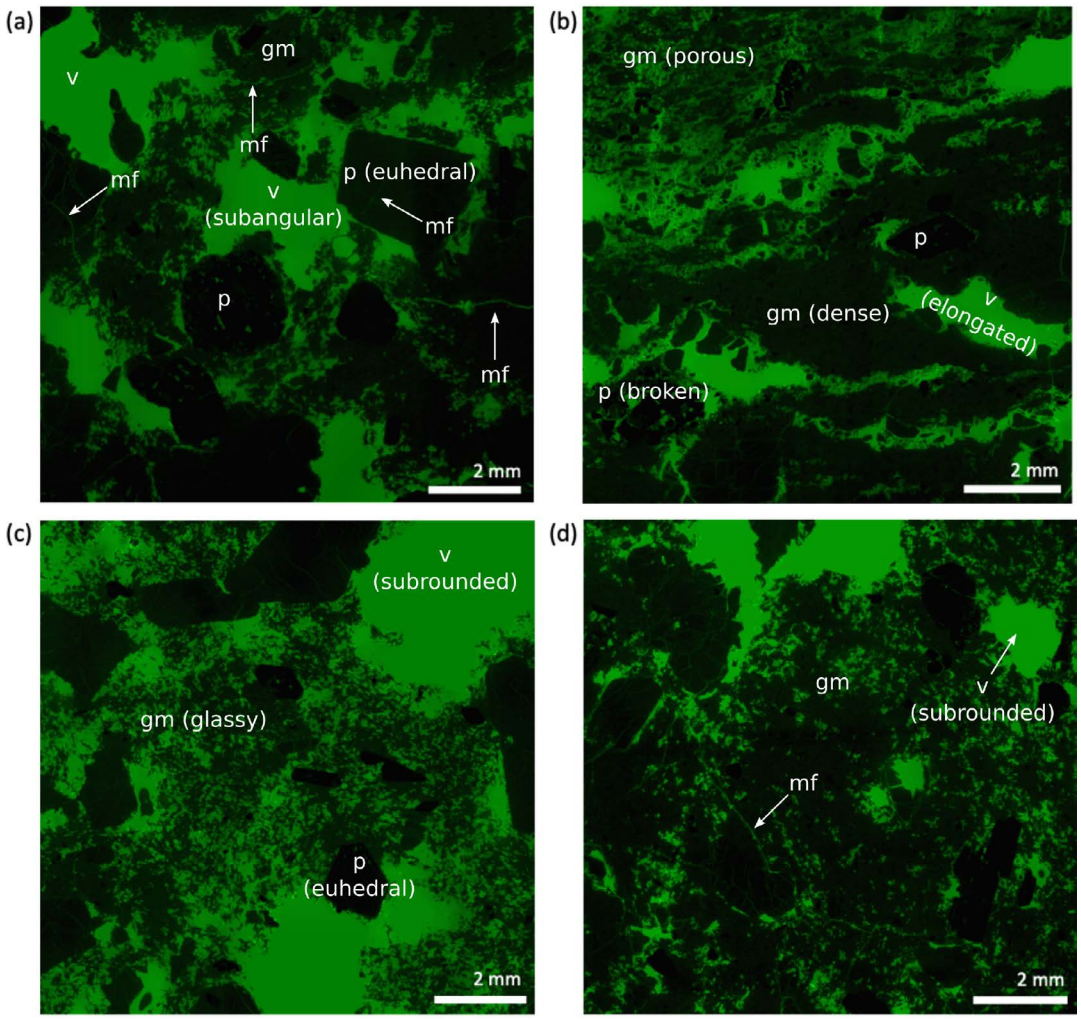

Figure 2 – Thin section images in reflected light with an ultraviolet filter, for each sample. **(a)** UNZ1 (ϕ = 18.6%) has isotropically distributed sub-angular vesicles and microfractures. Vesicles are typically adjacent to phenocrysts, and microfractures traverse both phenocrysts and groundmass. UNZ1 contains large (typically 1–2 mm or greater) euhedral phenocrysts; **(b)** UNZ9 (ϕ = 16.2%) has an anisotropic cataclastic fabric, composed of elongate, sub-angular pore space flanked by granular fault gouge including angular broken crystals and groundmass. Dense bands of more compacted groundmass run parallel to elongate porous bands. **(c)** UNZ13 (ϕ = 29%) has the highest porosity. The pores are large sub-rounded vesicles adjacent to phenocrysts and a finely vesicular glassy groundmass. Phenocrysts are typically euhedral, but smaller (typically 1-2 mm or less) than in sample UNZ1. **(d)** UNZ14 (ϕ = 13.4%) has the lowest porosity. The pores are typically sub-rounded, adjacent to phenocrysts, and smaller than in UNZ1 or UNZ13; a few short (<2 mm) microfractures are also in the groundmass. The phenocrysts are frequently broken and contain hairline fractures. gm = groundmass, mf = microfracture, p = phenocryst, v = vesicle.

required to ensure changes in strain were due primarily to earthquake loading and not load-hold induced brittle creep.

3.2.1 Load Hold (Time-Dependent Brittle Creep) Experiments

To determine the specimen's susceptibility to brittle creep, 24-hour stepped-load experiments at different percentages of the expected failure load were performed on one cylinder (compression) and one disk (tension) from each of the sample groups; UNZ1, UNZ9a, UNZ9b, UNZ13, and UNZ14 (10 tests total). Specimens were held under four load increments for six hours each: at 40% of expected failure load during Step 1, 50% during Step 2, 60% during Step 3, and 70% during Step 4 (Figure 3a). The expected failure load is assumed to be the average strength value of multiple strain-to-failure strength tests performed by *Kendrick et al.* (2021) on cores and disks from the same blocks as studied herein (Table 2). For each step, the load was applied at a rate of 1 MPa/min for compression and 0.5 MPa/min for tension until it reached the load hold condition, to approximately match the standard strain rate of 10-5 s^{-1} during load to failure testing applied in *Kendrick et al.* (2021). Stepped-load tests allowed us to determine the critical load, and hence stress, required to generate irreversible damage in the form of creep, which would be marked by appreciably higher rates of strain (Figure 3a). This, in turn, determined the maximum starting load below the critical load of brittle creep for the earthquake experiments, which ensures that damage measured during earthquake experiments is from earthquake loading and not brittle creep.

Table 1 – Height, diameter, connected porosity, and permeability of cored specimens from each block used in load hold and load oscillation experiments for this study. Connected porosity and permeability from *Kendrick et al.* (2021).

	Test	Block	Specimen	Height (mm)	Diameter (mm)	Connected porosity (%)	Permeability (m^2)
Load hold (brittle creep)	Compression	UNZ1	9	39.98	20.10	16.68	1.25×10^{-12}
		UNZ9a	6	40.26	20.15	12.64	6.68×10^{-14}
		UNZ9b	12	40.11	20.13	17.90	3.99×10^{-13}
		UNZ13	6	40.41	20.13	30.37	3.26×10^{-12}
		UNZ14	7	40.12	20.12	12.80	5.15×10^{-14}
	Tension	UNZ1	6	22.64	39.85	18.62	1.27×10^{-12}
		UNZ9a	3	21.95	39.77	16.75	5.20×10^{-14}
		UNZ9b	3	21.71	39.87	18.03	3.52×10^{-13}
		UNZ13	10	21.84	39.80	32.01	1.58×10^{-11}
		UNZ14	13	22.55	39.87	14.31	1.71×10^{-13}
Load oscillation (earthquake)	Compression	UNZ1	3	39.83	20.09	18.47	1.71×10^{-12}
		UNZ9a	1	40.21	20.12	13.21	1.99×10^{-13}
		UNZ9b	2	40.49	20.12	14.73	1.54×10^{-14}
		UNZ13	4	39.81	20.07	29.12	4.73×10^{-13}
		UNZ14	5	39.77	20.12	14.15	6.59×10^{-13}
	Tension	UNZ1	8	21.39	39.83	18.14	1.78×10^{-12}
		UNZ9a	7	20.83	39.99	15.51	1.11×10^{-13}
		UNZ9b	2	20.60	39.84	20.18	1.03×10^{-13}
		UNZ13	11	21.73	39.82	33.90	4.41×10^{-11}
		UNZ14	1	22.41	39.87	14.04	1.07×10^{-13}

Table 2 – Average uniaxial compressive and tensile strength of blocks used in this study as reported in *Kendrick et al.* (2021). As the tests are destructive, strength was determined on different specimens than were used in this study. Load hold conditions for our tests were calculated based on these average strength values, with Steps 1–4 being approximately 40%, 50%, 60%, and 70% of the average strength, respectively. MPa: megapascals; std. dev.: standard deviation.

Test	Block	No. of specimens	Average strength (MPa) ± std. dev.	Average connected porosity (%) ± std. dev.	Calculated load-hold conditions (MPa)			
					Step 1	Step 2	Step 3	Step 4
Compression	UNZ1	3	17.69 ± 0.49	18.55 ± 1,76	7.07	8.84	10.61	12.38
	UNZ9a	3	31.12 ± 1.98	15.39 ± 1,76	13.22	15.42	18.67	21.78
	UNZ9b	3	22.99 ± 11.86	16.99 ± 3.34	9.20	11.49	13.79	16.09
	UNZ13	3	21.38 ± 7.05	28.99 ± 3.67	8.76	10.22	12.83	14.97
	UNZ14	3	44.81 ± 2.65	13.43 ± 0.84	18.85	21.29	26.88	31.36
Tension	UNZ1	3	1.90 ± 0.24	18.74 ± 2.23	0.78	0.98	1.17	1.36
	UNZ9a	3	1.80 ± 0.68	14.41 ± 5.25	0.72	0.90	1.08	1.26
	UNZ9b	3	3.39 ± 0.40	15.98 ± 5.42	1.36	1.70	2.04	2.38
	UNZ13	3	2.01 ± 0.16	32.33 ± 2.35	0.80	1.00	1.12	1.36
	UNZ14	3	3.01 ± 0.60	14.06 ± 0.91	1.12	1.40	1.55	1.78

3.2.2 Load Oscillation (Earthquake) Experiments

To determine the specimens' susceptibility to damage from earthquake events, we conducted dynamic tests, subdivided by steps in Figure 3b. In Step 1, the specimen is loaded at a rate of 1 MPa/min for compression and 0.5 MPa/min for tension until it reaches 60% of its expected failure load, which we selected from the load-hold tests described in Section 3.2.1. Performing experiments at 60% of a sample's expected failure load is above the threshold stress required for dilatant microcracking, or where axial stress begins non-linearly decreasing as a function of axial strain (referred to as C'; *Heap et al.*, 2009), as calculated from uniaxial compressive strength tests from (*Kendrick et al.*, 2021) (see Table SI-1, Supporting Information). This ensures that the rock is above the point of elastic and recoverable damage, but below a brittle creep rate that progresses at a rate measurable in the laboratory test times as seen from the load-hold tests. In Step 2, the specimen is held for 30 minutes at this load (60% of its expected failure load) to determine if the specimen experiences brittle creep prior to testing. While stepped load hold tests are conducted on specimens from each block (as explained in Section 3.2.1), each specimen has slight heterogeneities, so this ensures that measured damage is from earthquake load oscillation and not due to brittle creep. In Step 3, we subject the specimen to 21 earthquake events spaced two minutes apart, with the earthquake spacing being similar to rhythmic seismicity measured at Unzen volcano by *Lamb et al.* (2015). To simulate stress variations as-

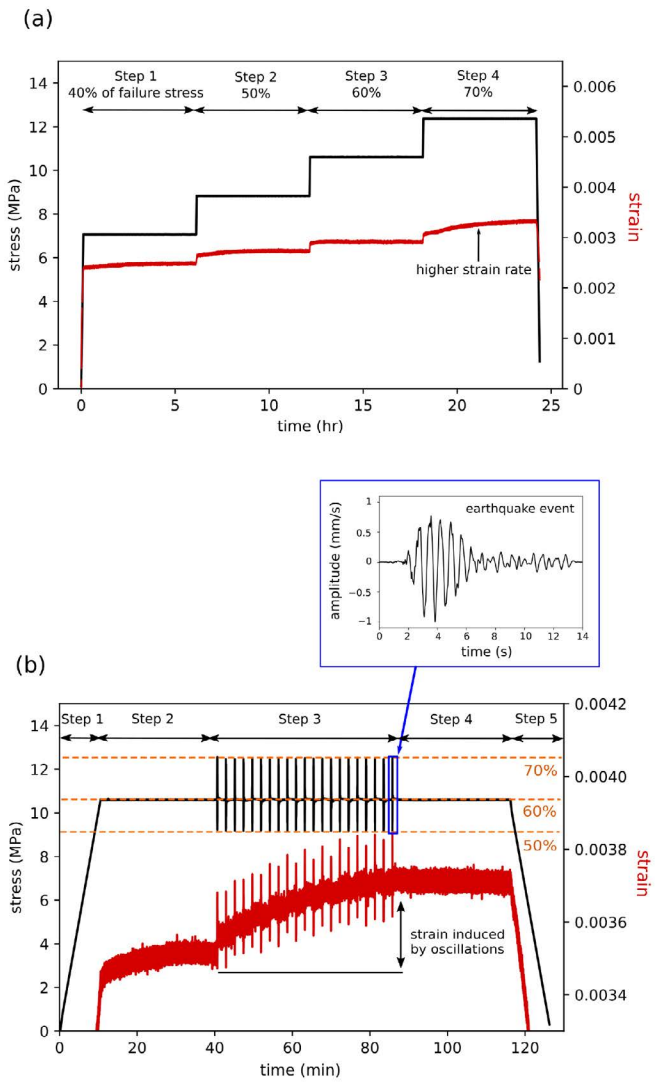

Figure 3 – Example load hold and load oscillation test. **(a)** A representative load hold test in compression showing the applied variations in stress (black line) and resulting variations in strain (red line) during a stepped-load brittle creep experiment. Specimens were held for six hours during each step, which increased from 40% to 70% of strength (from *Kendrick et al.*, 2021, see values in Table 2). The example shown is sample UNZ1 under compressive stress. **(b)** A representative load oscillation test, which mimics volcanic material subjected to repetitive earthquakes, showing the applied variations in stress (black line) and resulting variations in strain (red line; note the vertical axis is cropped). In Step 1, the sample is loaded to 60% of its strength based on uniaxial compressive strength tests, where it is held for 30 minutes in Step 2. Step 3 then subjects the rock to 21 earthquake events spaced 2 minutes apart, with the load change being 50% and 70% of each specimens' strength. The inset shows the amplitude over time of the earthquake, which is a 14-s stacked earthquake cluster event from a magma intrusion at Unzen in 1994 from *Lamb et al.* (2015). Step 4 again holds the rock for 30 minutes at 60% of its expected failure load, until the specimen is unloaded in Step 5. The difference in strain from the first to the last hold, accumulated during the oscillation period, is permanent strain, or damage, on the rock. The example shown is sample UNZ1 under compressive stress. See supplementary Figure S2 for a zoomed view of successive earthquake events.

sociated with earthquakes, the Instron WaveMatrix software was used to cycle the stress applied to the sample, resulting in a motion of the lower piston position, simulating longitudinal stress (i.e., compression and dilation) of multiple seismic waves while the specimen is under a load. These stress pulses may represent either proximal small events, or distal large magnitude earthquakes. Mt. Unzen is subject to both earthquake types; *Miyano et al.* (2021) measured 7,600 earthquakes within a 100 by 100 km area centered on the volcano between 2002 and 2020. Additionally, larger and more distal earthquake events are possible, such the 2016 Kumamoto earthquake (*Kato et al.*, 2016). Here, the stress fluctuation replicates a 14-second stacked earthquake cluster event from the extrusion of the lava spine at Unzen in 1994 (Figure 3b inset; *Lamb et al.*, 2015). The maximum amplitude of the waveform correlates to the maximum stress fluctuation (±10% from holding load at 60% of the strength) and is scaled for each different materials' strength in both compression and tension. This resulted in strains of 10^{-6}–10^{-5} for compression tests and 10^{-3} for tension. In Step 4, the sample was left to creep for 30 minutes at 60% of its expected failure load, to assess the resultant mechanical response following the earthquake sequence. The sample was then unloaded at a rate of 1 MPa/min for compression and 0.5 MPa/minute for tension in Step 5.

4 Results

4.1 Load Hold (Time-Dependent Brittle Creep) Results

Average strain (mean absolute strain during a given step) and strain rate (or equivalent diametric strain for indirect tensile experiments), calculated in each load-hold step for both compression and tension experiments are shown in Figure 4. For each strain and strain rate estimate, we also calculate the associated standard error (see Tables SI-2 and SI-3, Supporting Information). As expected, strain generally increases as the applied stress increases. UNZ1 and UNZ14 experienced the most strain in compression, whereas UNZ1, UNZ9b, and UNZ14 experienced the most strain in tension. Strain rate is relatively stable when held at 40, 50, and 60% of strength, but becomes appreciably faster at 70% of strength for sample UNZ9b. UNZ9b ultimately failed in both compression and tension while at 70% of the strength determined in *Kendrick et al.* (2021). Thus, a value of 60% of the strength was used for the hold value in load oscillating earthquake tests.

4.2 Load Oscillation (Earthquake) Results

Earthquake experiments show that total strain typically increases during each successive earthquake event (Figures 5 and 6). In tension, average strain rates appear to modulate, which is a function of the instrument precision at very low strain values; how-

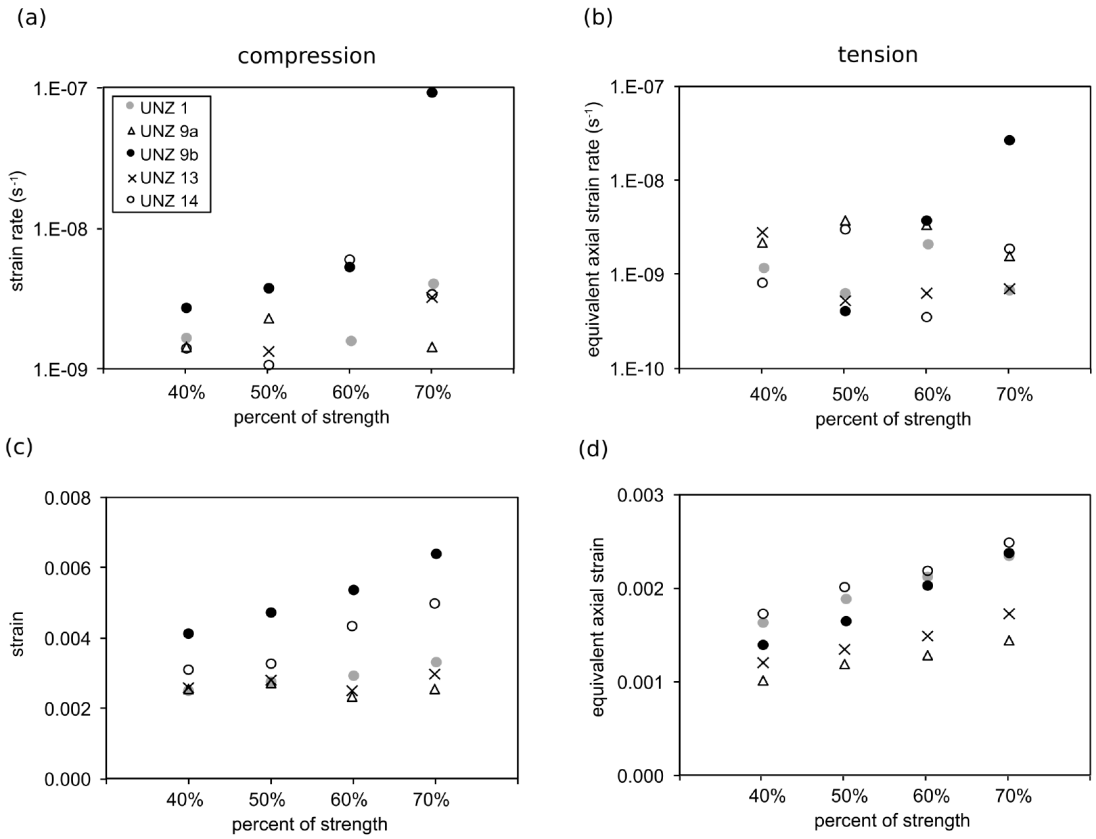

Figure 4 – Average strain rate and average strain during each step of the load hold experiments for the five sample groups; UNZ1, UNZ9a, UNZ9b, UNZ13 and UNZ14. **(a)** Average strain rate during each step in compression, **(b)** average strain rate during each step in tension **(c)** average strain during each step in compression, and **(d)** average strain during each step in tension. UNZ9b experienced a substantial increase in strain rate in both compression and tension at 70% of the material strength. Strain and strain rate were averaged over the final hour during each hold period; for UNZ9b, averages were determined for one hour ending 5 minutes prior to failure. Note that the symbol for UNZ1 at 70% of strength falls partially behind the UNZ9b symbol in (d).

ever, total strain increases in general with successive earthquake events. The strain rate is generally faster during intermittent stressing by earthquake events compared to the strain rate prior to the oscillations (Figure 7a–b); all samples in compression showed a marked acceleration, whereas three out of the five in tension showed substantial acceleration, and two out of the five samples remained relatively stable. In both compression and tension, strain accumulation (damage) is generally more pronounced in the first 5–8 earthquakes, which then reduces for subsequent earthquakes (in other words, each successive earthquake induces a smaller increase in strain than the previous one; Figures 5 and 6). Each specimen shows permanent strain, quantified as inelastic strain accumulated between the first hold (pre-earthquakes) and last hold (post-earthquakes) in earthquake oscillation tests (Figures 5 and 6). However, the amount of permanent strain accumulated during the intermittent oscillation regime (from the end of the first load-hold period to the start of the final load hold period, indicated in Figure 3b) varied between samples (Figure 7c–f). UNZ1, which has an intermediate porosity and is the most fracture-dominated block (Table 1 and Figure 2), experienced the most strain due to earthquake oscillations in both compression and tension (Figure 7c–d). In tension, UNZ1 failed following the 8th earthquake event when the change in strain was over 10%. This experiment showed an appreciable acceleration in strain rate during and between the three earthquake events prior to failure (Figures 5 and 6). UNZ1 also experienced the highest strain rate in compression during the earthquake oscillation phase (Figure 5), although it did not fail (Figure 7a–b). UNZ13, which is the most vesicle-dominated block, accumulated the least amount of strain in compression and the second lowest in tension despite having the highest porosity, whereas UNZ14 which has the lowest porosity, accumulated the least strain during the oscillation phase in tension (Figure 7). UNZ9a and UNZ9b experienced comparatively moderate strain compared to other samples in compression (Figure 6). In tension, UNZ9a experienced the least amount of strain and UNZ9b experienced the second highest strain (Figure 6).

5 Discussion

Time-dependent brittle creep experiments show that specimens generally increase in strain with each stepped load but do not typically experience strain rate increases within each step when held at or below 70% of strength. The failure of UNZ9b in both tension and compression during creep at 70% of the

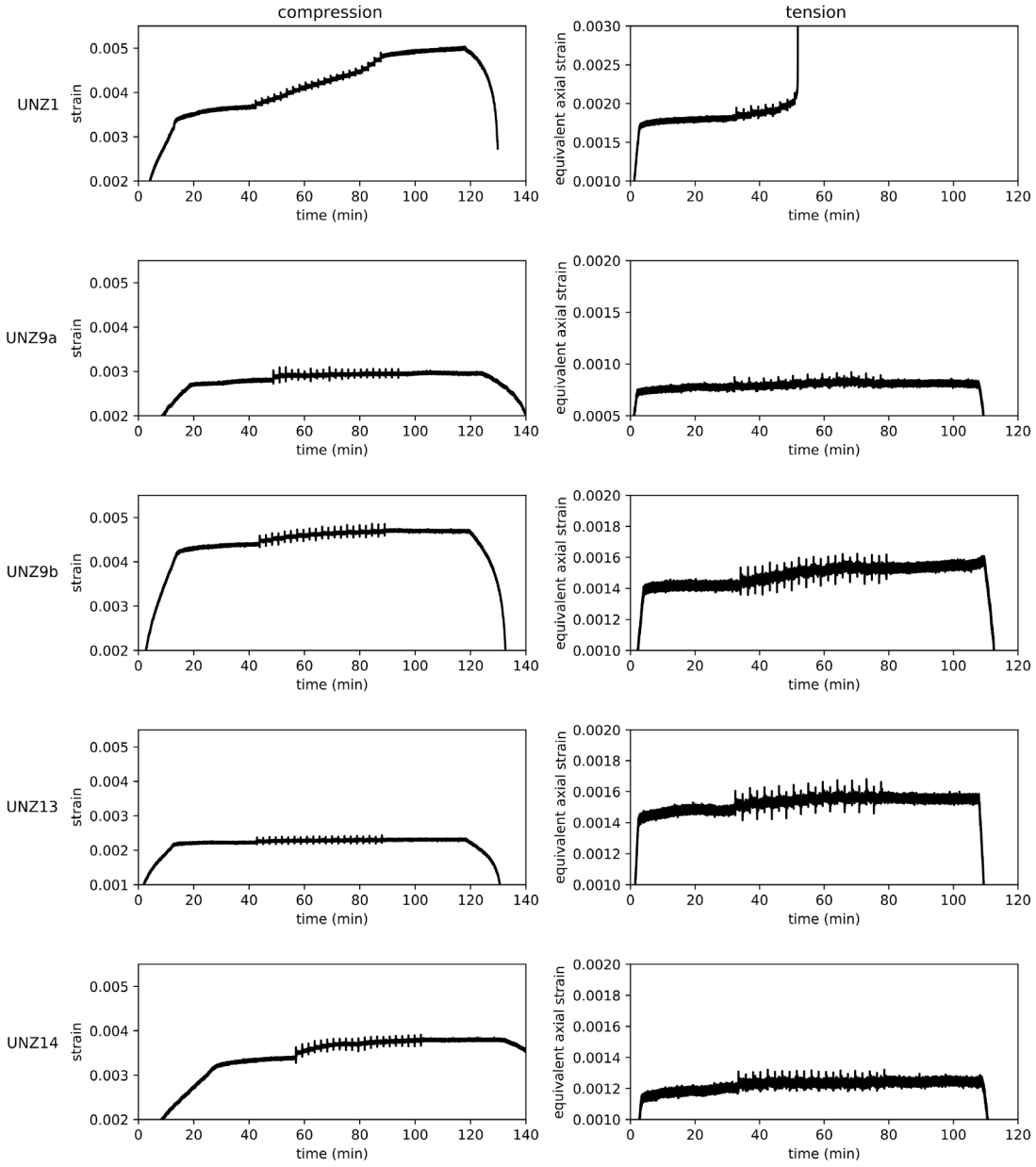

Figure 5 – Load oscillation test results in compression and tension for samples UNZ1, UNZ9a, UNZ9b, UNZ13, and UNZ14. The plots show the evolution of strain (or diametric equivalent strain in tension) for the samples subjected to stress oscillations. In most cases, strain rate is more rapid during the oscillation period (steeper slope) than during the creep at constant load and leads to accumulation of permanent strain (see annotated Figure 3b). Following the end of the oscillation period, the creep rate closely approximates the pre-oscillation rates. Note cropping of vertical axis to show details of earthquake events; all experiments begin at minute 0 and a strain of 0.

strength indicates that banded or anisotropic rocks may be more prone to failure during creep. This observation is in line with *Kendrick et al.* (2021), who found these banded cataclastic samples were susceptible to strain localization during loading, which increased their chance of unpredictable failure. However, UNZ9a, which was also foliated but cut in such a way that the bands were parallel to the principal applied stress in both compression and tension (see Figure SI-1, Supporting Information), did not fail in either compression or tension. Thus, the orientation of the banding influences the likelihood of failure. The Unzen dome contains multiple shear zones of varying structural importance *Wallace et al.* (e.g., 2019), has highly heterogeneous lava textures at the micrometer (e.g., microfracture density) to meter scale (e.g., structural fractures; Figure 1e, Figure 2; *Wallace et al.*, 2019), and has numerous shallow structural elements (e.g., *Hashimoto et al.*, 2020). If oriented unfavorably (e.g., dips with the slope), rock fabric or heterogenous structures may make the dome more prone to failure.

Load oscillation experiments demonstrate that oscillation events that simulate earthquakes bring rock specimens under quasi-uniaxial stress conditions (near-surface, partially confined) closer to failure; samples experience faster strain rates during intermittent stress oscillations, and all specimens had higher strain values after earthquake events, representing the accumulation of permanent inelastic

strain (Figure 7). Repetitive stressing of volcanic rock from successive earthquakes, which might occur during repeated intrusions, pulsatory dome growth (e.g., rhythmic seismicity during spine extrusion at Unzen; *Lamb et al.*, 2015, 2017), or in tectonically or volcanically active environments (e.g., *Miyano et al.*, 2021) can thus damage and reduce rock strength. This has additionally been shown for andesitic rock undergoing stress oscillations (*Lamur et al.*, 2023) and in volcanic rocks with cyclic mechanical stressing (e.g., *Heap et al.*, 2009; *Kendrick et al.*, 2013; *Schaefer et al.*, 2015). Slope stability analyses using reduced strengths for these mechanically weaker rocks indicate a propensity for failure, which can reduce slope stability by ~20% (*Donnadieu et al.*, 2001; *Reid et al.*, 2010).

In our experiments, we observed a jump in strain after the first earthquake oscillation, and then higher strain accumulation for the first 6–8 events, similar to *Lamur et al.* (2023), with successive events imparting less damage in cases that did not lead to wholesale sample failure. Rapid damage accumulation, demonstrated by higher rates of accumulated strain during initial earthquake events, emphasizes the immediate impacts of earthquake damage to rock. The reduction in strain accumulated in successive events in most of our tests also demonstrates that progressive development of the microfracture network may be restrained by the crack damage stress threshold (e.g., *Eberhardt et al.*, 1999). Although most samples did not fail catastrophically, permanent damage in the form of increased inelastic strain indicates that earthquake events can damage rock and promote instability over time in crucial zones. The longer-term effects of earthquake damage in our sample suite appear to be controlled by both rock anisotropy and whether a rock is fracture or pore dominated. The cataclastic banded sample UNZ9 suffered highly variable amounts of permanent strain in compression and tension in the two cored orientations (UNZ9a and UNZ9b), which we posit results from the relative contribution of compaction of the porous, fractured band in the different orientations (cf. *Farquharson et al.*, 2017; *Kendrick et al.*, 2021). In the more isotropic samples, UNZ1, which is the most fracture dominated sample and has microfractures traversing both phenocrysts and groundmass (Figure 2), experienced the most strain in the oscillation tests in compression and failed in tension (Figures 5-7). In both compression and tension, the amount of strain accumulated in each successive event began to increase again after the initial decrease, which in tension led to sample failure (Figure 6). UNZ1 notably had the lowest strength in compression and second lowest in tension (Table 2 *Kendrick et al.*, 2021) despite having intermediate porosity, which *Kendrick et al.* (2021) proposed showed the importance of pore geometry in defining rocks' susceptibility to accumulate damage during stressing, and therefore strength. In comparison, UNZ13, which has large, sub-rounded pores (Figure 2), experienced much lower permanent strain, particularly in tension (Figures 5 and 7), despite having the highest porosity (Table 1). Although a larger number of experiments would be useful to reduce uncertainty related to inherent sample-to-sample variability, we suggest that unsaturated, porous material can more efficiently buffer seismic energy due to pore compaction, as has been observed in other volcanic materials (*Andrews et al.*, 2007; *Lockner and Morrow*, 2008).

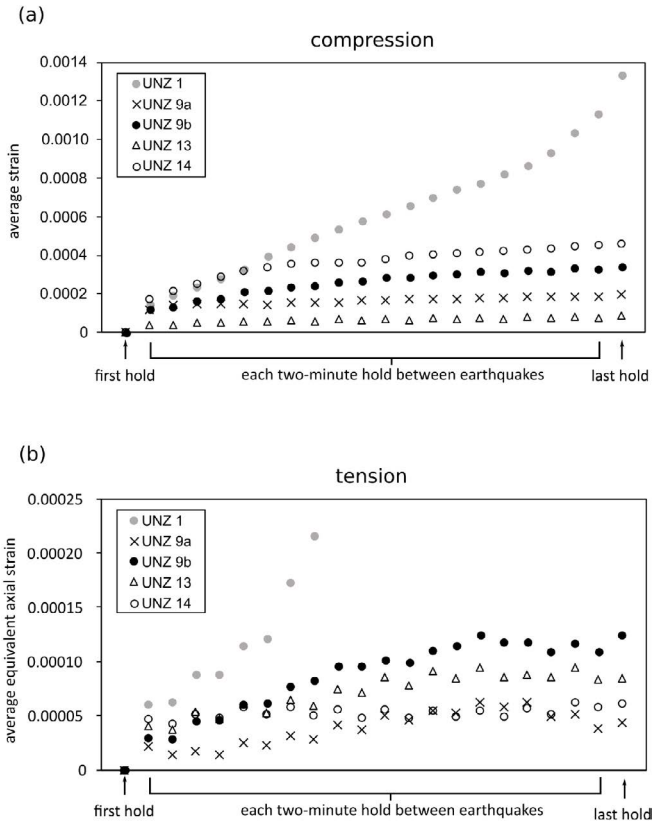

Figure 6 – Average accumulated strain for each experiment step including the first load hold (averaged over the final 5–10 minutes of the hold), each two-minute hold between oscillations (averaged over 100 seconds), and the last load hold for samples (averaged over the first 10 minutes of the hold) in **(a)** compression and **(b)** tension. Each experiment shows more prominent damage caused by the first ~6–8 earthquakes. UNZ1 accumulated high levels of damage after each successive earthquake and failed following the 8th earthquake in tension.

Our results reinforce the importance of microstructural variations (e.g., pores versus microfractures), or anisotropy on material strength and in defining rocks susceptibility to damage accumulation. Identifying rock masses at field-scale with adverse characteristics could thus be used to indicate zones more prone to landslide susceptibility during earthquake shaking. Oscillation experiments by *Lamur et al.* (2023) on andesitic volcanic rock also show that the amplitude of oscillations slightly correlates with the total amount of inelastic strain experienced by the rock, with samples subjected to larger amplitudes tending to record higher total accumulated strains after the final straining event. Defining the oscillation stress amplitude and resulting damage to material at various depths (increasing confinement), and how microstructures

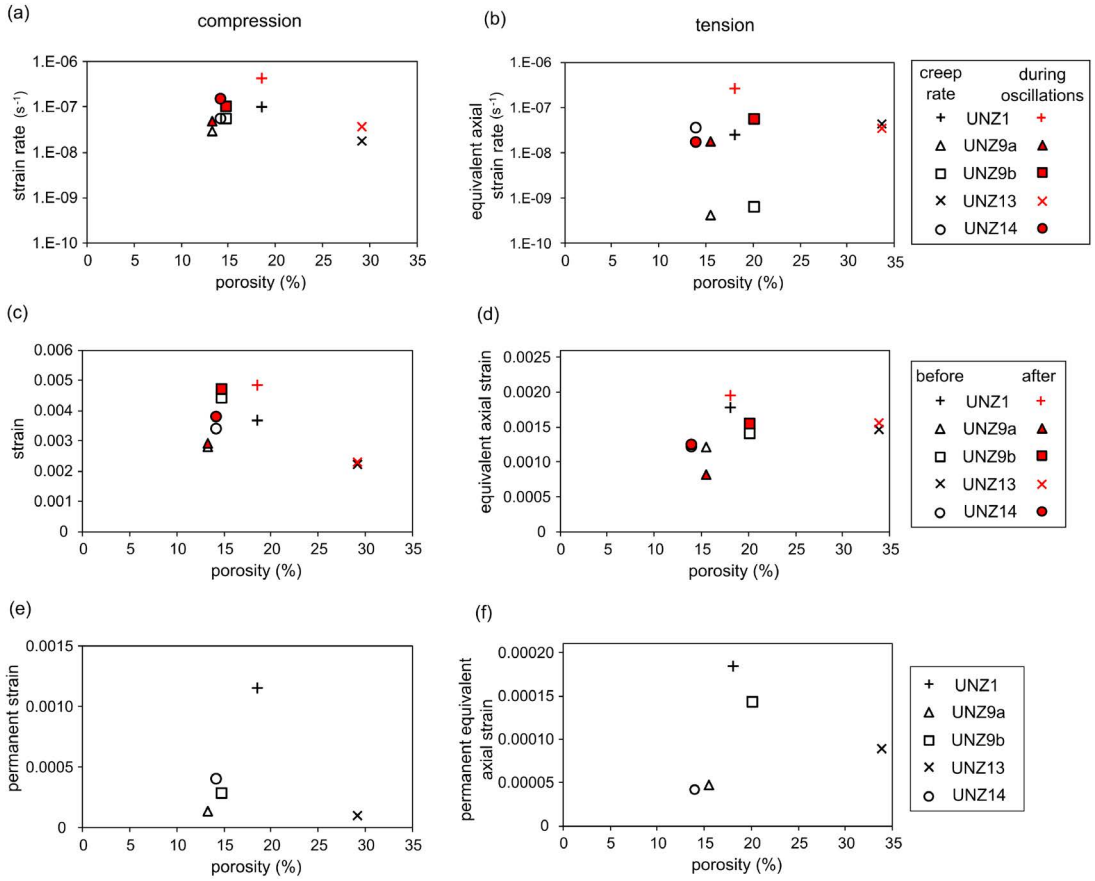

Figure 7 – Creep strain rate during a stable 5- to 10-minute period of the first load hold step in the oscillation tests, compared to the average strain rate throughout the phase of periodic stress oscillations for samples UNZ1, UNZ9a, UNZ9b, UNZ13, and UNZ14 in **(a)** compression and **(b)** tension. Inelastic, non-reversible strain imparted onto the samples by the stress oscillations can be assessed via the last measured strain before the first oscillation, and the first measured strain after the final oscillation, shown as "before" and "after", respectively, in **(c)** compression and **(d)** tension (see the schematic, Figure 3). The sample indicated by the black arrow failed following the 8th earthquake; therefore, the "after" strain is during the inter-earthquake hold period prior to the 8th oscillation. The difference between these "before" and "after" values is the permanent strain, shown in **(e)** in compression and **(f)** in tension plotted against sample porosity.

control this damage, would be informative further research avenues.

For domes experiencing creep, such as in the case of the Unzen dome (*Kohashi et al.*, 2012), the failure of sample UNZ1 demonstrates that repetitive loading events can prompt sufficient changes to materials to expedite a partially confined (near-surface) creeping rock to failure. This is supported by observations of earthquake-induced landslides (*Keefer*, 1984; *Rodríguez et al.*, 1999; *Inoue*, 1999). The acceleration in strain rate leading to failure after load-oscillation events may be measurable using geodetic methods in near real time (e.g., *Casagli et al.*, 2010) and used as an indicator of imminent catastrophic failure after earthquake events (e.g., *Intrieri et al.*, 2018). Although defining thresholds of rock mass failure is challenging, deformation monitoring and nonlinear fatigue damage cumulative models, applicable for both constant and variable loading conditions (*Xiao et al.*, 2009), may be used to define the transition from a uniform velocity phase (creep) to an accelerated phase.

6 Conclusion

Rock strength is a fundamental factor governing volcano stability at any scale. Dynamic processes such as gravity-driven brittle creep or earthquakes can damage and reduce rock strength at various time scales, with implications for landslides and other collapse events. This study examines the accumulation of damage in lava dome rocks from Unzen volcano, Japan, during time-dependent brittle creep and load oscillation earthquake simulation experiments. We observe that both the type of stressing event (load-hold or load oscillation, in both tension and compression) and the physical properties of the material, including porosity and pore geometry (vesicles or microfractures) as well as loading direction with respect to anisotropic fabrics, control the resulting degree of damage, and that damage varies over time and with subsequent loading events. Specifically, we find that rocks experience additional permanent strain, quantified as inelastic strain, following a period of oscillatory loading events compared to stable load. During periods of intermittent oscillatory loading to simulate earthquakes, strain rate is faster than during creep. Additionally, we showed that damage im-

parted is more prominent during initial load oscillation events and reduces with subsequent oscillations unless a sample exceeds a critical threshold, beyond which strain accumulation accelerates towards failure. Our results suggest fracture-dominated samples may be more susceptible to oscillation-induced strain than vesicle-dominated samples in both compression and tension. For banded, anisotropic rocks, orientation with respect to loading direction dictates the magnitude of strain accumulation under load oscillations. These experimental insights have important implications for determining damage accumulation of rock masses during stressing events and for monitoring volcanic stability. Additionally, our laboratory experiments show that damage during earthquake activity may in some cases increase rock susceptibility to wholesale rupture, which could generate landslides.

Acknowledgements

The authors would like to thank Takeshi Matsushima and Hiroshi Shimizu for their support and guidance. LNS, BK, JEK, and AL would like to acknowledge funding support from the Royal Society Te Apārangi Marsden project "Shaking magma to trigger volcanic eruptions." JEK was additionally funded by an Early Career Fellowship of the Leverhulme Trust (ECF-2016-325). YL, JS, AL, and OL acknowledge funding from the European Research Council (ERC) Starting Grant on "Strain Localisation in Magma" (SLiM no. 306488). YL acknowledges a Consolidator Grant from the European Research Council (ERC) on Magma outgassing during Eruptions and Geothermal Exploration (MODERATE, no. 101001065). YL and AL acknowledge financial support from a NERC grant (NE/T007796/1). This research project/publication was supported by LMU excellent, funded by the Federal Ministry of Education and Research (BMBF) and the Free State of Bavaria under the Excellence Strategy of the Federal Government and the Länder. Any use of trade, firm, or product names is for descriptive purposes only and does not imply endorsement by the U.S. Government.

Author contributions

JEK, **TM**, and **YL** collected the samples. **LNS** and **JEK** designed and carried out the experiments. **JS** prepared the samples and conducted physical measurements with **AL**, **JEK**, and **LNS**. **ODL** provided the seismic data. **LNS**, **JEK**, **ODL**, and **AL** processed the data. **LNS** and **JEK** prepared the tables and figures. **LNS** wrote the original draft. All authors contributed to the reviewing and editing of the article.

Data availability

Experimental data are available at: (https://doi.org/10.5066/P94CMZVO). The additional figures cited in the text can be found in the Supporting Information (https://tektonika.online/index.php/home/article/view/10/18).

Competing interests

The authors declare no competing interests.

Peer review

This publication was peer-reviewed by Michael Heap and Holly Unwin. The full peer-review report can be found here: https://tektonika.online/index.php/home/article/view/10/19k

Copyright notice

References

Almberg, L. D., J. F. Larsen, J. C. Eichelberger, T. A. Vogel, and L. C. Patino (2008), Comparison of eruptive and intrusive samples from unzen volcano, japan: Effects of contrasting pressure–temperature–time paths, *Journal of Volcanology and Geothermal Research*, *175*(1), 60–70, doi: 10.1016/j.jvolgeores.2008.03.020.

Andrews, D. J., T. C. Hanks, and J. W. Whitney (2007), Physical limits on ground motion at yucca mountain, *Bulletin of the Seismological Society of America*, *97*(6), 1771–1792, doi: 10.1785/0120070014.

ASTM (2014), Standard test methods for compressive strength and elastic moduli of intact rock core specimens under varying states of stress and temperatures, *Tech. Rep. ASTM Standard D7012-14e1*, American Society for Testing and Materials (ASTM), doi: 10.1520/D7012-14E01.

ASTM (2016), Standard test method for splitting tensile strength of intact rock core specimens, *Tech. Rep. ASTM Standard D3967–08*, American Society for Testing and Materials (ASTM), doi: 10.1520/D3967-08.

Attewell, P. B., and I. W. Farmer (1973), Fatigue behaviour of rock, *International Journal of Rock Mechanics and Mining Sciences & Geomechanics Abstracts*, *10*(1), 1–9, doi: 10.1016/0148-9062(73)90055-7.

Ball, J. L., P. H. Stauffer, E. S. Calder, and G. A. Valentine (2015), The hydrothermal alteration of cooling lava domes, *Bulletin of Volcanology*, *77*(12), 102, doi: 10.1007/s00445-015-0986-z.

Bell, A. F., S. Hernandez, J. McCloskey, M. Ruiz, P. C. LaFemina, C. J. Bean, and M. Möllhoff (2021), Dynamic earthquake triggering response tracks evolving unrest at sierra negra volcano, galápagos islands, *Science advances*, *7*(39), eabh0894, doi: 10.1126/sciadv.abh0894.

Belousov, A. B. (1995), The shiveluch volcanic eruption of 12 november 1964—explosive eruption provoked by failure of the edifice, *Journal of Volcanology and*

Geothermal Research, *66*(1), 357–365, doi: 10.1016/0377-0273(94)00072-O.

Borgia, A., L. Ferrari, and G. Pasquarè (1992), Importance of gravitational spreading in the tectonic and volcanic evolution of mount etna, *Nature*, *357*(6375), 231–235, doi: 10.1038/357231a0.

Brantut, N., M. J. Heap, P. G. Meredith, and P. Baud (2013), Time-dependent cracking and brittle creep in crustal rocks: A review, *Journal of Structural Geology*, *52*, 17–43, doi: 10.1016/j.jsg.2013.03.007.

Brenguier, F., M. Campillo, T. Takeda, Y. Aoki, N. M. Shapiro, X. Briand, K. Emoto, and H. Miyake (2014), Earthquake dynamics. mapping pressurized volcanic fluids from induced crustal seismic velocity drops, *Science*, *345*(6192), 80–82, doi: 10.1126/science.1254073.

Calder, E. S., R. Luckett, R. S. J. Sparks, and B. Voight (2002), Mechanisms of lava dome instability and generation of rockfalls and pyroclastic flows at soufrière hills volcano, montserrat, *Geological Society, London, Memoirs*, *21*(1), 173–190, doi: 10.1144/GSL.MEM.2002.021.01.08.

Casagli, N., F. Catani, C. Del Ventisette, and G. Luzi (2010), Monitoring, prediction, and early warning using ground-based radar interferometry, *Landslides*, *7*(3), 291–301, doi: 10.1007/s10346-010-0215-y.

Cerfontaine, B., and F. Collin (2018), Cyclic and fatigue behaviour of rock materials: Review, interpretation and research perspectives, *Rock Mechanics and Rock Engineering*, *51*(2), 391–414, doi: 10.1007/s00603-017-1337-5.

Coats, R., J. E. Kendrick, P. A. Wallace, T. Miwa, A. J. Hornby, J. D. Ashworth, T. Matsushima, and Y. Lavallée (2018), Failure criteria for porous dome rocks and lavas: a study of mt. unzen, japan, *Solid earth*, *9*(6), 1299–1328, doi: 10.5194/se-9-1299-2018.

Cordonnier, B., K.-U. Hess, Y. Lavallee, and D. B. Dingwell (2009), Rheological properties of dome lavas: Case study of unzen volcano, *Earth and planetary science letters*, *279*(3), 263–272, doi: 10.1016/j.epsl.2009.01.014.

Diederichs, M. S. (2003), Manuel rocha medal recipient rock fracture and collapse under low confinement conditions, *Rock Mechanics and Rock Engineering*, *36*(5), 339–381, doi: 10.1007/s00603-003-0015-y.

Donnadieu, F., O. Merle, and J.-C. Besson (2001), Volcanic edifice stability during cryptodome intrusion, *Bulletin of Volcanology*, *63*(1), 61–72, doi: 10.1007/s004450000122.

Eberhardt, E., D. Stead, and B. Stimpson (1999), Quantifying progressive pre-peak brittle fracture damage in rock during uniaxial compression, *International Journal of Rock Mechanics and Mining Sciences*, *36*(3), 361–380, doi: 10.1016/S0148-9062(99)00019-4.

Enescu, B., K. Shimojo, A. Opris, and Y. Yagi (2016), Remote triggering of seismicity at japanese volcanoes following the 2016 m7.3 kumamoto earthquake, *Earth, Planets and Space*, *68*(1), 1–9, doi: 10.1186/s40623-016-0539-5.

Farías, C., and D. Basualto (2020), Reactivating and calming volcanoes: The 2015 M W 8.3 illapel megathrust strike, *Geophysical research letters*, *47*(16), doi: 10.1029/2020gl087738.

Farquharson, J. I., P. Baud, and M. J. Heap (2017), Inelastic compaction and permeability evolution in volcanic rock, *Solid earth*, *8*(2), 561–581, doi: 10.5194/se-8-561-2017.

Fujita, E., T. Kozono, H. Ueda, Y. Kohno, S. Yoshioka, N. Toda, A. Kikuchi, and Y. Ida (2013), Stress field change around the mount fuji volcano magma system caused by the tohoku megathrust earthquake, japan, *Bulletin of Volcanology*, *75*(1), 679, doi: 10.1007/s00445-012-0679-9.

Hashimoto, T. M., K. Aizawa, Y. Hayashida, Y. Yuasa, T. Matsushima, Y. Yamamoto, K. Tsukamoto, K. Miyano, S. Matsumoto, and H. Shimizu (2020), Joint seismological–magnetotelluric investigation of shallow and implosive non-DC and DC earthquakes beneath the gravitationally unstable Heisei-Shinzan lava dome, unzen volcano, japan, *Journal of Volcanology and Geothermal Research*, *406*, 107,066, doi: 10.1016/j.jvolgeores.2020.107066.

Heap, M. J., and M. E. S. Violay (2021), The mechanical behaviour and failure modes of volcanic rocks: a review, *Bulletin of Volcanology*, *83*(5), 33, doi: 10.1007/s00445-021-01447-2.

Heap, M. J., S. Vinciguerra, and P. G. Meredith (2009), The evolution of elastic moduli with increasing crack damage during cyclic stressing of a basalt from mt. etna volcano, *Tectonophysics*, *471*(1), 153–160, doi: 10.1016/j.tecto.2008.10.004.

Hirakawa, Y., N. Usuki, K. Fujita, T. Tanaka, M. Kaneko, T. Ueno, H. Eguchi, and K. Shimokubo (2018), Monitoring system of a large rockslide in Heisei-Shinzan lava dome, mt. unzen, japan, in *Symposium Proceedings of the INTERPRAENENT 2018 in the Pacific Rim*.

Hornby, A. J., J. E. Kendrick, O. D. Lamb, T. Hirose, S. De Angelis, F. W. von Aulock, K. Umakoshi, T. Miwa, S. Henton De Angelis, F. B. Wadsworth, K.-U. Hess, D. B. Dingwell, and Y. Lavallée (2015), Spine growth and seismogenic faulting at mt. unzen, japan, *Journal of Geophysical Research, [Solid Earth]*, *120*(6), 4034–4054, doi: 10.1002/2014jb011660.

Hornby, A. J., Y. Lavallée, J. E. Kendrick, S. De Angelis, A. Lamur, O. D. Lamb, A. Rietbrock, and G. Chigna (2019), Brittle-ductile deformation and tensile rupture of dome lava during inflation at santiaguito, guatemala, *Journal of Geophysical Research, [Solid Earth]*, *124*(10), 10,107–10,131, doi: 10.1029/2018jb017253.

Inoue, K. (1999), Shimabara-Shigatusaku earthquake and topographic changes by shimabara catastrophe in 1792, *Journal of the Japan Society of Erosion Control Engineering*, *52*(4), 45–54, doi: 10.11475/sabo1973.52.4_45.

Intrieri, E., F. Raspini, A. Fumagalli, P. Lu, S. Del Conte, P. Farina, J. Allievi, A. Ferretti, and N. Casagli (2018), The maoxian landslide as seen from space: detecting precursors of failure with sentinel-1 data, *Landslides*, *15*(1), 123–133, doi: 10.1007/s10346-017-0915-7.

Kato, A., K. Nakamura, and Y. Hiyama (2016), The 2016 kumamoto earthquake sequence, *Proceedings of the Japan Academy. Series B, Physical and biological sciences*, *92*(8), 358–371, doi: 10.2183/pjab.92.359.

Keefer, D. K. (1984), Landslides caused by earthquakes, *GSA Bulletin*, *95*(4), 406–421, doi: 10.1130/0016-7606(1984)95<406:LCBE>2.0.CO;2.

Kendrick, J. E., R. Smith, P. Sammonds, P. G. Meredith, M. Dainty, and J. S. Pallister (2013), The influence of thermal and cyclic stressing on the strength of rocks from mount st. helens, washington, *Bulletin of Volcanology*, *75*(7), 728, doi: 10.1007/s00445-013-0728-z.

Kendrick, J. E., L. N. Schaefer, J. Schauroth, A. F. Bell, O. D. Lamb, A. Lamur, T. Miwa, R. Coats, Y. Lavallée, and B. M. Kennedy (2021), Physical and mechanical rock properties of a heterogeneous volcano: the case of mount unzen, japan, *Solid Earth*, *12*(3), 633–664, doi: 10.5194/se-12-633-2021.

Kerr, R. A. (1984), Landslides from volcaooes seen as common: Given the example of mount st. helens' catastrophic collapse, geologists are recognizing volcanic debris avalanches elsewhere, *Science*, *224*(4646), 275–276, doi: 10.1126/science.224.4646.275.

Klein, E., and T. Reuschlé (2004), A pore crack model for the mechanical behaviour of porous granular rocks in the brittle deformation regime, *International Journal of Rock Mechanics and Mining Sciences*, *41*(6), 975–986, doi: 10.1016/j.ijrmms.2004.03.003.

Kohashi, S., S. Shimokawa, K. Shimizu, Y. Satohira, T. Yamada, and T. Kimura (2012), Document for the committee of survey and countermeasure on lava dome collapse in unzen volcano (in japanese), *Tech. rep.*, Shimabara-shi Uto-cho.

Kueppers, U., B. Scheu, O. Spieler, and D. B. Dingwell (2005), Field-based density measurements as tool to identify preeruption dome structure: set-up and first results from unzen volcano, japan, *Journal of Volcanology and Geothermal Research*, *141*(1), 65–75, doi: 10.1016/j.jvolgeores.2004.09.005.

Lamb, O. D., S. De Angelis, K. Umakoshi, A. J. Hornby, J. E. Kendrick, and Y. Lavallée (2015), Repetitive fracturing during spine extrusion at unzen volcano, japan, *Solid earth*, *6*(4), 1277–1293, doi: 10.5194/se-6-1277-2015.

Lamb, O. D., S. De Angelis, R. J. Wall, A. Lamur, N. R. Varley, G. Reyes-Dávila, R. Arámbula-Mendoza, A. J. Hornby, J. E. Kendrick, and Y. Lavallée (2017), Seismic and experimental insights into eruption precursors at volcán de colima, *Geophysical research letters*, *44*(12), 6092–6100, doi: 10.1002/2017GL073350.

Lamur, A., J. E. Kendrick, L. N. Schaefer, Y. Lavallée, and B. M. Kennedy (2023), Damage amplification during repetitive seismic waves in mechanically loaded rocks, *Scientific reports*, *13*(1), 1271, doi: 10.1038/s41598-022-26721-x.

Lavallée, Y., and J. E. Kendrick (2021), Chapter 5 - a review of the physical and mechanical properties of volcanic rocks and magmas in the brittle and ductile regimes, in *Forecasting and Planning for Volcanic Hazards, Risks, and Disasters*, vol. 2, edited by P. Papale, pp. 153–238, Elsevier, doi: 10.1016/B978-0-12-818082-2.00005-6.

Lesage, P., G. Reyes-Dávila, and R. Arámbula-Mendoza (2014), Large tectonic earthquakes induce sharp temporary decreases in seismic velocity in volcán de colima, mexico, *Journal of Geophysical Research, [Solid Earth]*, *119*(5), 4360–4376, doi: 10.1002/2013jb010884.

Liu, Y., and F. Dai (2021), A review of experimental and theoretical research on the deformation and failure behavior of rocks subjected to cyclic loading, *Journal of Rock Mechanics and Geotechnical Engineering*, *13*(5), 1203–1230, doi: 10.1016/j.jrmge.2021.03.012.

Lockner, D. A., and N. M. Beeler (2002), 32 - rock failure and earthquakes, in *International Geophysics*, vol. 81, edited by W. H. K. Lee, H. Kanamori, P. C. Jennings, and C. Kisslinger, pp. 505–537, Academic Press, doi: 10.1016/S0074-6142(02)80235-2.

Lockner, D. A., and C. A. Morrow (2008), Energy dissipation in calico hills tuff due to pore collapse, in *2008 AGU Fall Meeting*, vol. 2008, pp. T51A–1856.

Marone, C. (1998), LABORATORY-DERIVED FRICTION LAWS AND THEIR APPLICATION TO SEISMIC FAULTING, *Annual review of earth and planetary sciences*, *26*(1), 643–696, doi: 10.1146/annurev.earth.26.1.643.

Matsushima, T., and A. Takagi (2000), GPS and EDM monitoring of unzen volcano ground deformation, *Earth, Planets and Space*, *52*(11), 1015–1018, doi: 10.1186/BF03352323.

Miyabuchi, Y. (1999), Deposits associated with the 1990–1995 eruption of unzen volcano, japan, *Journal of Volcanology and Geothermal Research*, *89*(1), 139–158, doi: 10.1016/S0377-0273(98)00129-2.

Miyano, K., K. Aizawa, T. Matsushima, A. Shito, and H. Shimizu (2021), Seismic velocity structure of unzen volcano, japan, and relationship to the magma ascent route during eruptions in 1990-1995, *Scientific reports*, *11*(1), 22,407, doi: 10.1038/s41598-021-00481-6.

Nakada, S., and Y. Motomura (1999), Petrology of the 1991–1995 eruption at unzen: effusion pulsation and groundmass crystallization, *Journal of Volcanology and Geothermal Research*, *89*(1), 173–196, doi: 10.1016/S0377-0273(98)00131-0.

Nakada, S., H. Shimizu, and K. Ohta (1999), Overview of the 1990–1995 eruption at unzen volcano, *Journal of Volcanology and Geothermal Research*, *89*(1), 1–22, doi: 10.1016/S0377-0273(98)00118-8.

Paterson, M. S., and T.-F. Wong (2005), *Experimental Rock Deformation - The Brittle Field*, 2 ed., Springer Berlin Heidelberg, doi: 10.1007/b137431.

Reid, M. E., T. E. C. Keith, R. E. Kayen, N. R. Iverson, R. M. Iverson, and D. L. Brien (2010), Volcano collapse promoted by progressive strength reduction: new data from mount st. helens, *Bulletin of Volcanology*, *72*(6), 761–766, doi: 10.1007/s00445-010-0377-4.

Rodŕıguez, C. E., J. J. Bommer, and R. J. Chandler (1999), Earthquake-induced landslides: 1980–1997, *Soil Dynamics and Earthquake Engineering*, *18*(5), 325–346, doi: 10.1016/S0267-7261(99)00012-3.

Rutter, E. H. (1986), On the nomenclature of mode of failure transitions in rocks, *Tectonophysics*, *122*(3), 381–387, doi: 10.1016/0040-1951(86)90153-8.

Saito, H., S. Uchiyama, Y. S. Hayakawa, and H. Obanawa (2018), Landslides triggered by an earthquake and heavy rainfalls at aso volcano, japan, detected by UAS and SfM-MVS photogrammetry, *Progress in Earth and Planetary Science*, *5*(1), 1–10, doi: 10.1186/s40645-018-0169-6.

Sato, H., T. Fujii, and S. Nakada (1992), Crumbling of dacite dome lava and generation of pyroclastic flows at unzen volcano, *Nature*, *360*(6405), 664–666, doi: 10.1038/360664a0.

Satou, Y., T. Ishizuka, S. Kuraoka, and Y. Nakashima (2014), Deformation characteristics of unzen lava dome based on long range displacement monitoring, in *Proceedings of 2014 INTERPREAEVENT International Symposium*, pp. 25–28.

Schaefer, L. N., J. E. Kendrick, T. Oommen, Y. LavallÃ©e, and G. Chigna (2015), Geomechanical rock properties of a basaltic volcano, *Frontiers of earth science*, *3*, doi: 10.3389/feart.2015.00029.

Schaefer, L. N., B. M. Kennedy, J. E. Kendrick, Y. Lavallée, and T. Miwa (2020), Laboratory measurements of damage evolution in dynamic volcanic environments: From slow to rapid strain events, *54th U.S. Rock Mechanics/Geomechanics Symposium*, pp. ARMA–2020–1876.

Scheu, B., U. Kueppers, S. Mueller, O. Spieler, and D. B. Dingwell (2008), Experimental volcanology on eruptive products of unzen volcano, *Journal of Volcanology and Geothermal Research*, *175*(1), 110–119, doi: 10.1016/j.jvolgeores.2008.03.023.

Scholz, C. H. (1968), The frequency-magnitude relation of microfracturing in rock and its relation to earthquakes, *Bulletin of the Seismological Society of America*, *58*(1), 399–415, doi: 10.1785/BSSA0580010399.

Scholz, C. H., and T. A. Koczynski (1979), Dilatancy anisotropy and the response of rock to large cyclic loads, *Journal of geophysical research*, *84*(B10), 5525, doi: 10.1029/jb084ib10p05525.

Schultz, R. A. (1995), Limits on strength and deformation properties of jointed basaltic rock masses, *Rock Mechanics and Rock Engineering*, *28*(1), 1–15, doi: 10.1007/BF01024770.

Shi, X., Y. Jiang, and Y. Hirakawa (2018), Growth and potential collapse of the lava dome in unzen volcano and the estimation on block-and-ash flows, *Geosciences Journal*, *22*(2), 273–286, doi: 10.1007/s12303-017-0051-3.

Thouret, J.-C., R. Salinas, and A. Murcia (1990), Eruption and mass-wasting-induced processes during the late holocene destructive phase of nevado del ruiz volcano, colombia, *Journal of Volcanology and Geothermal Research*, *41*(1), 203–224, doi: 10.1016/0377-0273(90)90089-X.

Voight, B. (2000), Structural stability of andesite volcanoes and lava domes, *Philosophical Transactions of the Royal Society of London. Series A: Mathematical, Physical and Engineering Sciences*, *358*(1770), 1663–1703, doi: 10.1098/rsta.2000.0609.

Voight, B., H. Glicken, R. J. Janda, and P. M. Douglass (1981), Catastrophic rockslide avalanche of may 18, in *The 1980 Eruptions of Mount St. Helens, Washington*, vol. 1250, edited by P. W. Lipman and D. R. Mullineaux, pp. 347–377, US Geological Survey, doi: 10.3133/pp1250.

Wallace, C. S., L. N. Schaefer, and M. C. Villeneuve (2021), Material properties and triggering mechanisms of an andesitic lava dome collapse at shiveluch volcano, kamchatka, russia, revealed using the finite element method, *Rock Mechanics and Rock Engineering*, *55*(5), 2711–2728, doi: 10.1007/s00603-021-02513-z.

Wallace, P. A., J. E. Kendrick, T. Miwa, J. D. Ashworth, R. Coats, J. E. P. Utley, S. Henton De Angelis, E. Mariani, A. Biggin, R. Kendrick, S. Nakada, T. Matsushima, and Y. Lavallée (2019), Petrological architecture of a magmatic shear zone: A multidisciplinary investigation of strain localisation during magma ascent at unzen volcano, japan, *Journal of Petrology*, *60*(4), 791–826, doi: 10.1093/petrology/egz016.

Walter, T. R., R. Wang, M. Zimmer, H. Grosser, B. Lühr, and A. Ratdomopurbo (2007), Volcanic activity influenced by tectonic earthquakes: Static and dynamic stress triggering at mt. merapi, *Geophysical research letters*, *34*(5), doi: 10.1029/2006GL028710.

Walter, T. R., M. Haghshenas Haghighi, F. M. Schneider, D. Coppola, M. Motagh, J. Saul, A. Babeyko, T. Dahm, V. R. Troll, F. Tilmann, S. Heimann, S. Valade, R. Triyono, R. Khomarudin, N. Kartadinata, M. Laiolo, F. Massimetti, and P. Gaebler (2019), Complex hazard cascade culminating in the anak krakatau sector collapse, *Nature communications*, *10*(1), 4339, doi: 10.1038/s41467-019-12284-5.

Xiao, J.-Q., D.-X. Ding, G. Xu, and F.-L. Jiang (2009), Inverted s-shaped model for nonlinear fatigue damage of rock, *International Journal of Rock Mechanics and Mining Sciences*, *46*(3), 643–648, doi: 10.1016/j.ijrmms.2008.11.002.

Yamamoto, T., S. Takarada, and S. Suto (1993), Pyroclastic flows from the 1991 eruption of unzen volcano, japan, *Bulletin of Volcanology*, *55*(3), 166–175, doi: 10.1007/BF00301514.

Yates, A. S., M. K. Savage, A. D. Jolly, C. Caudron, and I. J. Hamling (2019), Volcanic, coseismic, and seasonal changes detected at white island (whakaari) volcano, new zealand, using seismic ambient noise, *Geophysical research letters*, *46*(1), 99–108, doi: 10.1029/2018gl080580.